1-D fluid model of atmospheric-pressure rf He+O2 cold plasmas: Parametric study and critical evaluation

Aijun Yang, Xiaohua Wang, Mingzhe Rong, Dingxin Liu, Felipe Iza et al.

Related Articles

Plasmon effects on the entanglement fidelity for elastic collisions in hot quantum plasmas
Phys. Plasmas 18, 114503 (2011)

Oscillatory quantum screening effects on the positronium (Ps) formation in quantum plasmas
Appl. Phys. Lett. 99, 191503 (2011)

A study of dust grain screening in a weakly ionized plasma based on the numerical solution of the Vlasov-Bhatnagar-Gross-Krook kinetic equations
Phys. Plasmas 18, 103707 (2011)

Charge exchange recombination spectroscopy for particles colliding with hydrogen atoms
Phys. Plasmas 18, 103301 (2011)

Head-on collision of dust acoustic solitary waves in a four-component dusty plasma with nonthermal ions
Phys. Plasmas 18, 103703 (2011)

Additional information on Phys. Plasmas

Journal Homepage: http://pop.aip.org/

Journal Information: http://pop.aip.org/about/about_the_journal

Top downloads: http://pop.aip.org/features/most_downloaded

Information for Authors: http://pop.aip.org/authors

1-D fluid model of atmospheric-pressure rf He+O$_2$ cold plasmas: Parametric study and critical evaluation

Aijun Yang,[1] Xiaohua Wang,[1] Mingzhe Rong,[1,a)] Dingxin Liu,[1] Felipe Iza,[2,b)] and Michael G. Kong[1,2]

[1]*State Key Laboratory of Electrical Insulation and Power Equipment, Xi'an Jiaotong University, Xi'an 710049, People's Republic of China*
[2]*School of Electronic, Electrical and Systems Engineering, Loughborough University, Loughborough LE11 3TU, United Kingdom*

In this paper atmospheric-pressure rf He+O$_2$ cold plasmas are studied by means of a 1-D fluid model. 17 species and 60 key reactions selected from a study of 250+ reactions are incorporated in the model. O$_2^+$, O$_3^-$, and O are the dominant positive ion, negative ion, and reactive oxygen species, respectively. Ground state O is mainly generated by electron induced reactions and quenching of atomic and molecular oxygen metastables, while three-body reactions leading to the formation of O$_2$ and O$_3$ are the main mechanisms responsible for O destruction. The fraction of input power dissipated by ions is ∼20%. For the conditions considered in the study ∼6% of the input power is coupled to ions in the bulk and this amount will increase with increasing electronegativity. Radial and electrode losses of neutral species are in most cases negligible when compared to gas phase processes as these losses are diffusion limited due to the large collisionality of the plasma. The electrode loss rate of neutral species is found to be nearly independent of the surface adsorption probability p for $p > 0.001$ and therefore plasma dosage can be quantified even if p is not known precisely. © *2011 American Institute of Physics*. [doi:10.1063/1.3655441]

I. INTRODUCTION

In recent years, atmospheric pressure plasmas have received growing attention due to lower-cost and easier implementation than their low-pressure counterparts. As a result, atmospheric pressure plasmas are being explored for a large variety of applications including plasma medicine,[1–3] air purification,[4,5] sterilization,[6,7] surface modification,[8,9] and water treatment.[10,11] Many of these applications rely on the production of reactive oxygen species (ROS), which can be obtained readily in atmospheric-pressure cold plasmas in gases containing admixtures of O$_2$ and/or H$_2$O. The electronegative character of O$_2$ and H$_2$O containing plasmas and their complex chemistry results in intricate plasma dynamics and chemical kinetics that are gradually being unraveled by growing number of experimental and computational studies.[12–18]

Accounting for a complete chemistry model in a fluid simulation is computational demanding and therefore simpler global models are often used to identify the main chemical pathways in the discharge. Global models determine volume-averaged quantities eliminating spatial gradients and reducing the computational cost.[14] Global models of low-temperature atmospheric-pressure plasmas in Ar+O$_2$, He+O$_2$ and He+H$_2$O have recently been reported.[15–18] Global models, however, are a crude approximation of the actual discharge because in most atmospheric-pressure plasmas local kinetics prevail and inhomogeneous spatio-temporal profiles are routinely observed experimentally.[19]

Fluid models are a better representation and have been used to study atmospheric-pressure electronegative discharges, revealing interesting features. For example, a DBD in He+O$_2$ mixtures was numerically studied with a model that accounted for 12 species and 18 reactions[20] and an RF-excited He+O$_2$ plasma jet using a more comprehensive chemistry model that incorporated 16 species and 116 reactions.[21] 2-D fluid models of He+O$_2$+H$_2$O plasmas have also been reported in the literature.[22]

In this paper we report on the simulation results of a He+O$_2$ (0.5%) rf (13.56 MHz) discharge at atmospheric-pressure by means of a 1D fluid model with a chemistry set that includes 17 species and 60 reactions (Table II). These have been identified as the main chemical species/reactions in a previous study that used a comprehensive chemistry model with 250+ reactions.[16] Besides the main 55 reactions identified in Refs. 16 and 5 additional reactions that were neglected due to the overestimation of the radial flux in the previous study[16] have been incorporated.

The paper is organized as follows. The model used in the study is described in detail in Sec. II and the simulation results are presented in Sec. III. In Secs. IV and V power distribution, and sidewise (radial) and electrode (axial) losses are discussed in detail and concluding remarks are given in Sec. VI.

II. DESCRIPTION OF THE MODEL

Fluid models have been widely used for the investigation of low-temperature atmospheric-pressure plasmas. Most of the models found in the literature are based on home-made codes, although a growing number of commercial

a)Electronic mail: mzrong@mail.xjtu.edu.cn.
b)Electronic mail: f.iza@lboro.ac.uk.

18, 113503-1

modeling platforms are being reported in recent years. For this study COMSOL Multiphysics® was used. This generic partial differential equation solver has successfully been used in other 1-D and 2-D plasma studies.[21,23,24]

The discharge considered in this study is generated between two circular electrodes with radius $R = 1$ cm, separated by a gap $g = 0.2$ cm. The plasma is rf excited (13.56 MHz) with an average power density of 40 W/cm^3. A He+O$_2$ (0.5%) mixture is used as feedstock gas, and the gas flow rate is assumed to be 1slm. The neutral gas temperature is set to be 350 K. These conditions reflect those encountered in the experimental work of Liu *et al.*[19] and are kept constant through the paper.

The plasma chemistry used in this study is based on the comprehensive analysis reported in Ref. 16 where the main species and dominant reactions in He+O$_2$ plasmas were selected out of 250+ reactions. In that study 3 regimes were identified based on the oxygen concentration in the background gas. The oxygen concentration considered in this study (0.5%) lies on the boundary of regime 2 and 3 identified in Ref. 16, and therefore for this work we have combined the reactions given for those two regimes. As a result the following species are considered in the model: electrons (e), positive ions (O$_2^+$, O$_4^+$), negative ions (O$^-$, O$_2^-$, O$_3^-$), electronic excited species (He*, He$_2$*, O(^{1}D), O(^{1}S), O$_2$(a$^1\Delta_g$), O$_2$(b$^1\sum_g^+$)), vibrational excited species (O$_2(\nu)$, $\nu = 1$–4), and ground state neutrals (He, O$_2$, O, and O$_3$). The 60 reactions considered in the model are listed in Table II in the Appendix.

The fluid model solves the mass conservation equation for each species (Eq. (1)), the current continuity equation (Eq. (2)) and the electron energy conservation equation (Eq. (3)). Given the high collisionality of the discharge, the particles inertia is neglected and the drift-diffusion approximation is used in the model (Eq. (4))

$$\frac{\partial n_i}{\partial t} + \nabla \cdot \mathbf{\Gamma}_i = S_i, \qquad (1)$$

$$\mathbf{J}(t) = \varepsilon_0 \frac{\partial \mathbf{E}}{\partial t} + \left(-e\mathbf{\Gamma}_e + e\sum \mathbf{\Gamma}_+ - e\sum \mathbf{\Gamma}_- \right), \qquad (2)$$

$$\frac{\partial n_e \varepsilon}{\partial t} + \nabla \cdot \left(\frac{5}{3} \varepsilon \mathbf{\Gamma}_e - \frac{5}{3} n_e D_e \nabla \varepsilon \right)$$
$$= -e\mathbf{\Gamma}_e \cdot \mathbf{E} - \sum_j \Delta E_j R_j - \sum_k 3 \frac{m_e}{m_k} R_{el,k} k_B (T_e - T_k), \qquad (3)$$

$$\mathbf{\Gamma}_i = \text{sgn}(q_i) n_i \mu_i \mathbf{E} - D_i \nabla n_i, \qquad (4)$$

where n_i, $\mathbf{\Gamma}_i$, μ_i, D_i, S_i, m_i are the density, flux, mobility, diffusion coefficient, net gain/loss rate and mass of species i. $\mathbf{J}$ is the net current density, $\mathbf{E}$ the electric field and ε the mean electron energy. ε_0 is vacuum permittivity, e the elementary charge and k_B the Boltzmann constant. R_{el} is the momentum transfer collisional rate between electrons and background gases and T the temperature of plasma species. ΔE_j and R_j are the electron energy loss due to inelastic collision j and its corresponding reaction rate. Subscripts e, $+$, $-$, and k represent electron, positive ion, negative ion and background gas species (He and O$_2$), respectively.

The gain/loss rate term (S_i) in Eq. (1), accounts not only for volume reactions but also for diffusion and advection in the radial direction, as these can become important in determining the density of long lived species, such as ozone, in He+O$_2$ plasmas

$$S_i = S_{r,i} - \Gamma_i s/V - F n_i / V, \qquad (5)$$

here $S_{r,i}$ is the net generation/loss rate of species i due to volume reactions in the plasma, Γ_i denotes the radial flux of species i due to diffusion, s the "sidewall" area ($2\pi Rg$), V the discharge volume ($\pi R^2 g$), F the gas flow rate and n_i the number density of species i. The second term on the right hand side ($\Gamma_i s/V$) represents the radial loss rate of species i due to diffusion, while the last term ($F n_i/V$) represents the radial loss rate of species i due to gas flow (advection). The radial loss can only be approximated in a 1D simulation and it is further discussed in Sec. IV.

Regarding fluxes to the electrodes, the following boundary conditions are used for charged species:

$$\mathbf{\Gamma}_e \cdot \mathbf{n} = -a\mu_e \mathbf{E} \cdot \mathbf{n} n_e + 0.25 v_{th,e} n_e - \gamma \sum_p \mathbf{\Gamma}_{+,p}, \qquad (6)$$

$$\mathbf{\Gamma}_+ \cdot \mathbf{n} = a\mu_+ \mathbf{E} \cdot \mathbf{n} n_+ + 0.25 v_{th,+} n_+, \qquad (7)$$

$$\mathbf{\Gamma}_- \cdot \mathbf{n} = -a\mu_- \mathbf{E} \cdot \mathbf{n} n_- + 0.25 v_{th,-} n_-, \qquad (8)$$

where $\mathbf{n}$ is the normal vector pointing towards the wall, γ is the secondary emission coefficient and v_{th} the thermal velocity. γ is set to 0.03 for positive ions and zero for other species, following the simplistic approach previously used by Shi *et al.*[25] A more accurate description of the secondary electron emission processes that accounts for metastable- and photon-induced electrons would be required for discharges operated in the gamma-mode (lower frequency, smaller gaps, higher input)[26–28] as under those conditions secondary processes can affect the discharge dynamics considerably.[29] The switching function α takes a value of one when the drift velocity is directed towards the electrode and zero otherwise:[30]

$$a = \begin{cases} 1, & \text{sgn}(q_i)\mu_i \mathbf{E} \cdot \mathbf{n} > 0 \\ 0, & \text{sgn}(q_i)\mu_i \mathbf{E} \cdot \mathbf{n} \le 0 \end{cases}. \qquad (9)$$

The electrode loss of neutral species is difficult to describe precisely as it may need to account for adsorption/desorption of species as well as surface reactions. The difficulty lies not in the modeling of these processes but on the lack of rate constants for most species and the dependence of these on the materials used as electrode/targets, their surface condition and even the exposure time to the plasma.[31] This loss is discussed in Sec. V.

The electron energy flux to the electrodes is given by[21,23]

$$\mathbf{\Gamma}_\varepsilon \cdot \mathbf{n} = \frac{5}{3}\left(\frac{1}{4}\varepsilon n_e v_{th,e} - \varepsilon_r \gamma \sum \mathbf{\Gamma}_+ \cdot \mathbf{n} \right), \qquad (10)$$

where ε_γ is the energy of secondary electron emitted from the electrodes and fixed at 5 eV.[23] The effective electron temperature (T_{eff}) is calculated from the electron mean

energy ($\varepsilon = 1.5 k_B T_{eff}$) and the ion temperature is obtained using Wannier's formulation.[32] The electron mobility and diffusivity are calculated as a function of mean electron energy using Bolsig+,[33] a Boltzmann solver. The transport coefficients for other species are obtained from the literature as summarized in Table I.

The set of equations described above is solved using a time-dependent finite-element partial differential equation solver, COMSOL Multiphysics®, and results have been post-processed with MATLAB®.

III. SIMULATION RESULTS

In order to validate the model, simulation results were first compared against experimental data. Fig. 1 shows the root-mean-square (RMS) I –V characteristic obtained in this study with the experimental data reported in Ref. 19. A reasonable agreement is found between the two, suggesting that the model is capable of capturing the main features of the discharge. Discrepancies between simulation and experimental data are mainly attributed to 2D effects not captured in the model (e.g., filling up of the discharge gap with increasing power) and the oversimplified account of secondary electron emission processes.

Fig. 2 shows the density profiles of electrons, positive ions, negative ions and net electrical charge, at 4 different times in an RF cycle. The ion density profiles remain virtually unchanged due to the large ion inertia, while the more mobile electrons oscillate between the two electrodes. The ambipolar field traps anions and confine them to the central region of the discharge, creating a central electronegative plasma core with electropositive edges. The ion density profiles are flat in the bulk and steep in the sheaths, as predicted for moderate-pressure electronegative discharges.[38] The preferential power deposition on the sheath edges during the expansion and contraction of the sheaths results on the observed double hump ionic profiles.[27] It is noted that the electronegativity (n_-/n_e) is around 1 even though the oxygen concentration is only 0.5%. Double layers typically observed
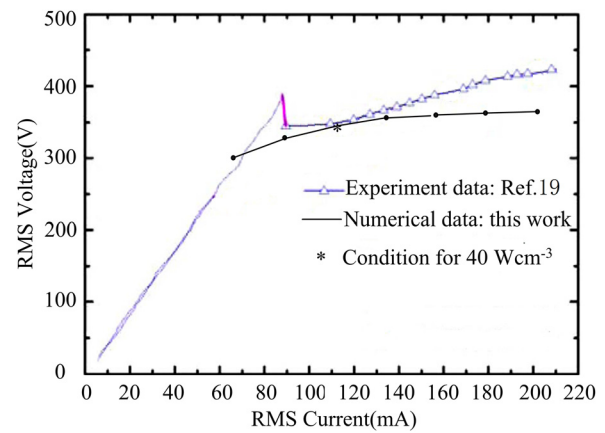

FIG. 1. (Color online) Comparison of the current–voltage curve predicted by the plasma model and experimental data from the literature.[19]

in electronegative discharges are also observable at the sheath-bulk boundaries in the net electrical charge profiles (curve IV in Fig. 2). These result from the modulation of the positive- and negative-ion densities at the sheath-bulk boundary.[39]

Fig. 3 shows the time-averaged spatial distributions of all the species considered in the model. The main cation is O$_2^+$, the main anion O$_3^-$, O is the main neutral species in ground state and O$_2$(a) the main excited neutral species. The plasma density is $\sim 10^{11}$ cm^{-3}, and for neutral species $[O] \approx 2 \times [O_2(a)] \approx 10 \times [O_3] \approx 1 \times 10^{16}$ cm^{-3}. Despite the abundance of helium in the discharge the density of He metastables are orders of magnitude smaller due to the rapid quenching by oxygen species (Penning ionization). These results agree well with experimental observations made in a comparable rf discharge by Ellerweg *et al.*[40] regarding the concentration of atomic oxygen and with the spatial profile reported by Waskoenig *et al.* using TALIF.[21] The results also agree with other studies that suggested that in He+O$_2$ (0.5%) discharges the O density is about one order of magnitude higher than that of ozone.[1] The density profiles of neutral species are similar to the charged species, but in the sheath they are less steep. Both the ambipolar field and the surface reactions affect charged species, but only the latter can directly influence the density of neutral species. Although not shown explicitly, it is noted that the density of the main ROS remain almost constant during one RF cycle due to their relatively long life time as compared to the RF period.

ROS are crucial for many atmospheric-pressure applications, particularly in plasma medicine where they are directly related to free radical biology.[41] Since atomic oxygen is the most abundant ROS (see Fig. 3(a)), it is worth examining its production mechanisms in more detail. Furthermore, atomic oxygen is also the main precursor for the formation of ozone (R57 in Table II), the longest lived ROS generated by the plasma which can have long range effects in application scenarios where the plasma is located remotely. As shown in Fig. 4(a), the dominant processes for the generation of O are O(^{1}D) quenching (mainly R44 and R58 in Table II), ozone dissociation by O$_2$(b) (R52-R53), and electron impact dissociation of O$_2$ (mainly R7). Dissociative attachment (R12) is

TABLE I. Transport coefficients (T in K).

Species	μ (cm^2 V^{-1} s^{-1})	D (cm^2/s)	Reference
O$_2^+$	22.4-2.4 $\times 10^{-3}$ T	a	32
O$_4^+$	67.1–7.0 $\times 10^{-3}$ T–38.3 $T^{0.03}$	a	b
O$^-$	85.9 $T^{-0.2}$	a	32
O$_2^-$	74.7 $T^{-0.22}$	a	32
O$_3^-$	51.8–18.3 $T^{-0.1}$	a	32
He*	—	1.64	34
He$_2$*	—	0.475	34
O	—	0.72	35
O(^{1}D)	—	0.72	35
O(^{1}S)	—	0.72	35
O$_2$(a)	—	0.698	36
O$_2$(b)	—	0.698	36
O$_2$(v)	—	0.698	36
O$_3$	—	0.698	37

^{a}Obtained from μ using the Einstein relation.
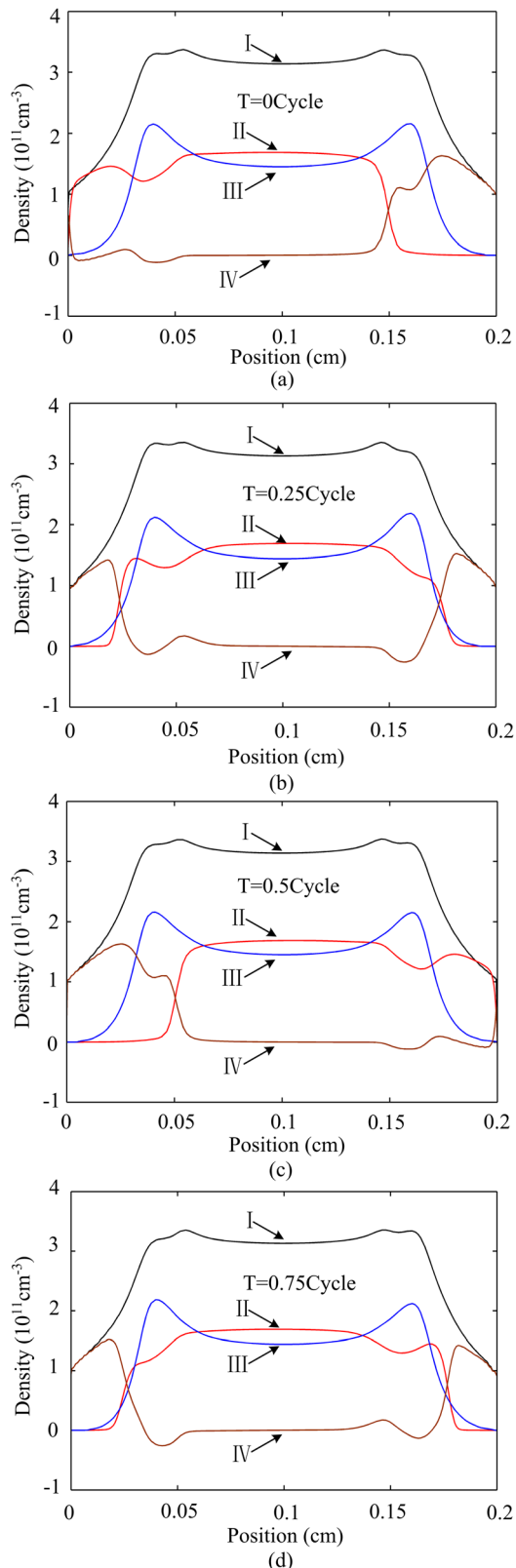^{b}Extrapolation from O$^+$ and O$_2^+$, Ref. 32.

FIG. 2. (Color online) Spatial distribution of positive ions (I), electron (II), negative ions (III), and net charge (IV) densities, at (a) t = 0, (b) t = 0.25τ_{rf}, (c) t = 0.50τ_{rf}, and (d) t = 0.75τ_{rf}, where τ_{rf} is the rf period (~74 ns).

found not to be important in the active plasma, although this process is expected to become significant in the afterglow.[42] The above processes account for ~99% of ground state O generation. Breaking the O-O bond requires >5.1 eV and
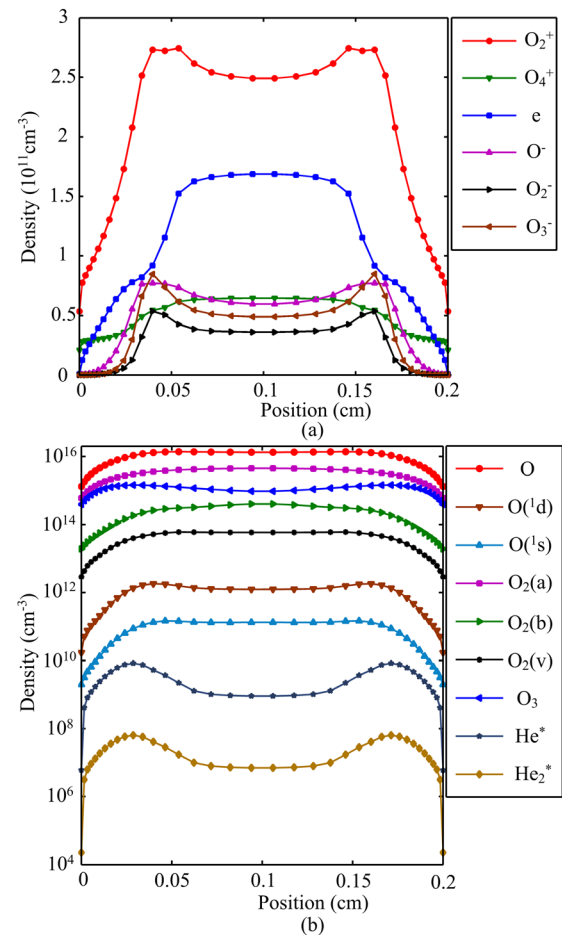

FIG. 3. (Color online) Time-averaged spatial distributions of (a) charged species and (b) neutral species.

therefore the main generation processes are directly or indirectly linked to energetic electrons. This implies that an increase in electron temperature will lead to higher efficacy of O production. Fig. 4(b) shows the main destruction processes of ground state O. These are dominated by recombination (R55) and ozone production (R57). Due to its large lifetime, ozone molecules can escape the discharge (radial and axial fluxes) with the rest being destroyed in the gas phase via collisions with O_2(b) (R52-53).

IV. POWER DISTRIBUTION

The input power is directly coupled to charged species in the discharge by accelerating them in the applied electric field. The energy gained by these species is then transferred via collisions to neutral species, resulting in excitation, generation of new plasma species, and heating of the background gas and electrodes. The time-averaged power density ($\mathbf{J}\cdot\mathbf{E}$) coupled to electrons, positive ions and negative ions are shown in Fig. 5. As expected, in the sheaths most of the power is coupled to positive ions that are accelerated against the electrodes. For the conditions of this study, 14.4% of the input power is coupled to ions and due to the collisional nature of the discharge most of this energy is transferred to the background gas, mitigating the ion bombardment of the electrode. On the contrary, in the bulk plasma the power is
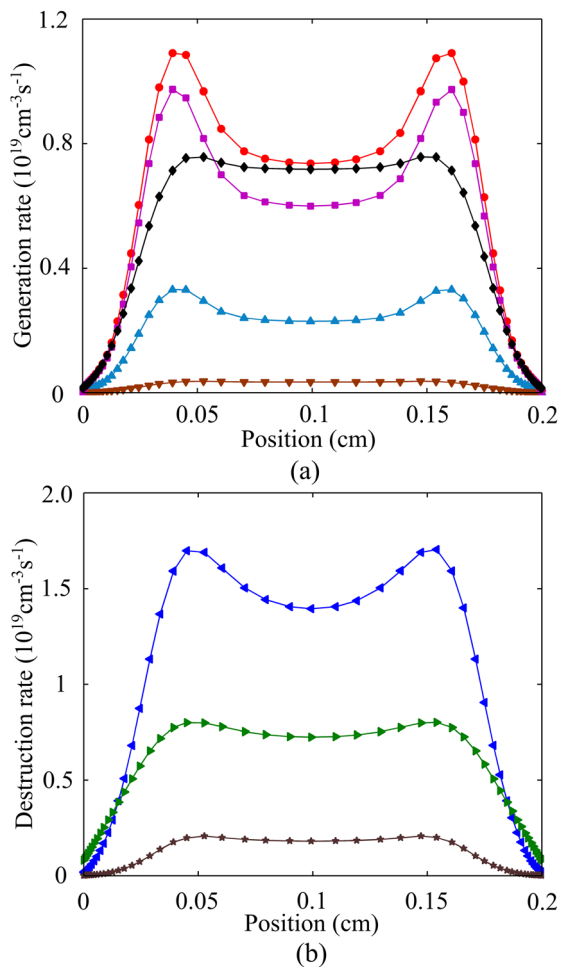
FIG. 4. (Color online) The main (a) generation processes and (b) destruction processes of ground state atomic oxygen O. ―●―: collisional relaxation of $O(^1D)$ (R42-R44, R58); ―■―: electron impact dissociative excitation (R7-R8); ―◆―: reaction between $O_2(b)$ and O_3 (R52-R53); ―▲―: electron impact dissociation (R6); ―▼―: other generation processes; ―◄―: recombination of ground state O via three-body reaction (R55); ―▶―: three-body reaction for O_3 formation (R57); ―★―: other destruction processes.

mainly coupled to the electrons, which carry most of the conduction current. Given the electronegative nature of the discharge, however, negative ions also contribute to this current and 3.1% of the input power is coupled to anions. Given the large collisionality of atmospheric-pressure plasmas (collision frequency $\gg$ rf frequency), the ratio of the power coupled to the electrons to the power coupled to the ions is given by the ratio of their mobilities. At atmospheric pressure ions have mobilities in the order of 10–20 cm² V⁻¹ s⁻¹ (see Table I) while electrons in the range of $\sim 10^3$ cm² V⁻¹ s⁻¹. Therefore in electropositive discharges where the electron and ion densities are equal, the power coupled to ions in the bulk plasma is typically <2%. In the bulk region of electronegative plasmas, however, because the ion-density is higher than the electron density, larger proportion of the input power is coupled to the ions. For example, in this study the electronegativity of plasma is around 1, which means the total ion density (anions and cations) is higher than the electron density by a factor of 3, and therefore in the bulk region approximately 6% of the input power is coupled to ions (see Fig. 5). At higher oxygen concentrations the discharge
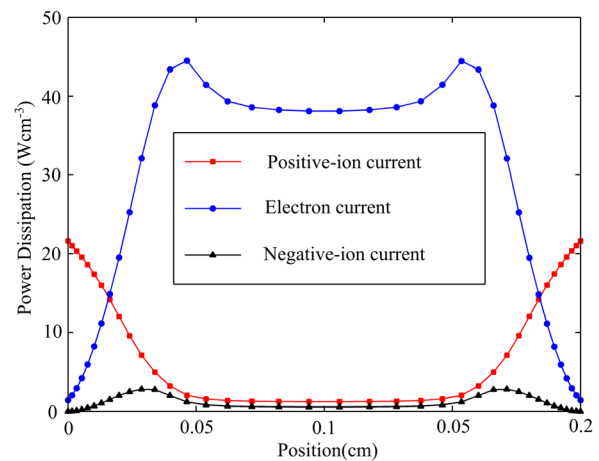

FIG. 5. (Color online) Spatial profile of the time-averaged power density dissipated by charged species.

becomes more electronegative and therefore the power coupling to the electrons will become increasingly less efficient. Increased attachment and reduced power coupling to the electrons lead to the decrease of the electron density as the oxygen concentration in the background gas and the discharge electronegativity increase.[43]

As discussed earlier, in He+O₂ plasmas the generation of ROS requires energetic electrons to initiate the reactions that lead to the formation of O and other reactive species (see Fig. 4(b)). Therefore although oxygen is required to generate ROS, once the discharge starts to become electronegative the decrease in electron density competes with the increasing oxygen content and eventually hinders the production of ROS. As a result He+O₂ plasmas are typically operated with reduced amount of oxygen and maximum process efficacy is often encountered at oxygen concentrations below 1%.[44,45]

In the last decades, global models have been used to study low-pressure electronegative plasmas[46–49] and in recent years these models have been extended to the study electronegative atmospheric-pressure discharges.[15–18] In these models it is customary to assume that the input power is mainly coupled to the electrons[50] with various approximations regarding the power coupled to ions in the sheath.[15,16,47] The power coupled to ions in the bulk, however, is normally neglected. As discussed in the previous paragraph, however, the power coupled to the ions in the bulk should be taken into account particularly as the electronegativity of the discharge increases above 1. For atmospheric pressure discharges, the amount of power coupled to ions can be estimated by mobility ratios and therefore it can be readily incorporated in global model calculations.

V. RADIAL AND AXIAL NEUTRAL FLUXES

The radial and axial fluxes of neutral species can affect the particle balance in the discharge but little studies have analyzed their influence in atmospheric pressure rf plasmas.

A. Radial losses

Radial losses may be important for the depopulation of long-lived species that are not readily quenched in the

plasma volume. Several studies have neglected radial loses without explicit justification[17,25,51] whereas others have assumed a thermal flux neglecting radial diffusion speed.[15] Here we derive analytical expressions that could be used to estimate these losses in global and 1-dimensional models and asses their relative importance in atmospheric pressure plasmas. Radial losses are due to diffusion ($S_{d,I} = \Gamma_i s/V$) and advection ($S_{f,I} = n_i F/V$) but since in a 1D model the radial density profile is not explicitly considered, an estimation of the radial fluxes based on the geometry and chemistry of the discharge is needed. Expressed in units of [$cm^{-3}\,s^{-1}$], radial and advection losses can be directly compared with the volume reaction rates that destroy neutral species in the plasma in order to assess their significance.

The mass conservation equation for long-lived species i is given by

$$\frac{dn_i(r,\varphi,z,t)}{dt} - D_i\nabla^2 n_i(r,\varphi,z,t) = S_{r,i}(r,\varphi,z,t). \quad (11)$$

Since the radial direction (r) is not solved for in the simulation, we aim at an approximated solution of Eq. (11) that could be used to estimate radial losses based on the density values at the centre of the discharge. The following assumptions are made in order to obtain an analytical solution:

1. The lifetime of the long-lived neutral species is much larger than the rf period and therefore its density can be considered independent of time. This is generally true for long-lived species in an rf plasma.
2. The density profile is axisymmetric. Depending on how the gas is fed into the discharge, the background flow could perturb the discharge symmetry. For the flow rate and geometry under consideration here, however, the advection loss rate is found to be negligible and therefore an axisymmetric profile is a save assumption.
3. The density profile along the axis of symmetry (i.e., across the gap) is approximated to be uniform. This is a reasonable approximation if one neglects the depleted areas near the electrodes (see Fig. 3(b)).
4. In order to obtain an analytical solution, it is also assumed that the generation rate is uniform in space.
5. Outside the electrode region plasma species are rapidly removed and therefore at $r=R$ the radial flux of species equals to the thermal flux, i.e., $-D\frac{dn}{dr}\big|_{r=R} = \frac{1}{4}n(R)v_{th}$.

With the assumptions above, Eq. (11) can be simplified to

$$-\frac{D}{r}\frac{d}{dr}\left(r\frac{dn(r)}{dr}\right) = S. \quad (12)$$

Let us first consider a limiting case of a species that is created with a rate G and that is not destroyed in the plasma, i.e., a long lived species that will be balanced solely by radial diffusion.

The solution to Eq. (12) in this case is

$$n(r) = n_o\left(1 - \frac{r^2}{R^2\left(1+\frac{8D}{Rv_{th}}\right)}\right), \quad (13)$$

where n_o is the density at r = 0. Therefore the radial loss as a function of the central density is given by

$$S_{d,i} = \frac{s}{V}\frac{1}{4}n_o\left(1 - \frac{1}{1+\frac{8D}{Rv_{th}}}\right)v_{th}. \quad (14)$$

If the "diffusion speed" (D/R) is much larger than the thermal velocity, the radial density profile becomes fairly flat and the radial flux due to diffusion approaches $\frac{1}{4}n_o v_{th}$. For parallel plate atmospheric pressure plasmas, however, D/R (~ 1 cm/s) tends to be much smaller than the thermal velocity ($\sim 10^4$ cm/s) and the density profile becomes parabolic with a much lower density on the edges than at the centre (see Fig. 6). In this case the radial losses are smaller than the thermal flux based on the central density.

For most species in the plasma, however, there will be reactions that destroy them in the gas phase and radial diffusion will not be the only destruction mechanism. As an example, let us consider ground state O, the most abundant ROS. With the assumptions listed above, Eq. (11) can be simplified for ground state O to

$$-\frac{D}{r}\frac{d}{dr}\left(r\frac{dn}{dr}\right) = G - Kn, \quad (15)$$

where G is the average generation rate (constant) due to gas phase reactions and K the reaction frequency for the destruction of O (linear approximation). Solution of Eq. (15) yields

$$n(r) = n_0\left[1 - \frac{0.25 v_{th}I_0\left(\sqrt{\frac{K}{D_i}}r\right)}{\sqrt{D_iK}\sum_{m=1}\frac{\left(\sqrt{\frac{K}{D_i}}R\right)^{2m-1}}{2^{2m}(m!)^2} + 0.25 I_0\left(\sqrt{\frac{K}{D_i}}R\right)v_{th}}\right], \quad (16)$$

where I_0 is the modified Bessel function of zero order. Equation (16) can then be used to determine the density at $r=R$ and the radial loss of plasma species
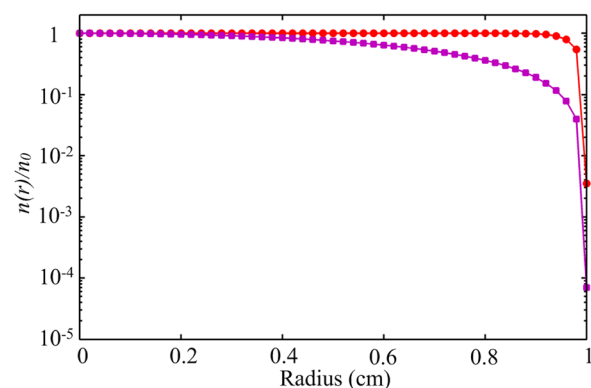

FIG. 6. (Color online) Comparison of the normalized ground state O density profile in the radial direction obtained with (—●—: Eq. (16)) and without (—■—: Eq. (13)) volume loss.

$$S_{d,i} = \frac{s}{V}\frac{1}{4}n_o\left[1 - \frac{0.25v_{th}I_0\left(\sqrt{\frac{K}{D_i}}r\right)}{\sqrt{D_iK}\sum\limits_{m=1}\frac{\left(\sqrt{\frac{K}{D_i}}R\right)^{2m-1}}{2^{2m}(m!)^2} + 0.25I_0\left(\sqrt{\frac{K}{D_i}}R\right)v_{th}}\right]v_{th}. \tag{17}$$

For ground state O, $G_i = 2.4 \times 10^{19}$ cm^{-3} s^{-1}, $K = 1050$ s^{-1}, $D_i = 0.72$ cm^2 s^{-1} and the resulting radial profile for O is shown in Fig. 6. As a result of the volume loss, the density profile flattens and for a given central density (n_o), larger density exists at the edge (r = R) when gas phase destruction exists. The radial diffusion loss rate for ground state O (Eq. (17)) is $S_{d,I} \sim 10^{16}$ cm^{-3} s^{-1}, about 3 orders of magnitude smaller than that of O in the gas phase reactions (Fig. 4(b)) and therefore radial diffusion loss of O can be neglected.

Similar analysis of the diffusion radial loss of the other neutral species in the plasma suggests that for the parallel plate configuration considered here, diffusion radial losses can be neglected for all the species except for ozone.

It is noted that we have assumed that species will be readily removed once they diffuse out of the plasma region. Ozone, however, is likely to build up in the atmosphere surrounding the plasma if the gas is not actively circulated. If ozone is allowed to build up, the boundary condition for the solution of Eq. (11) will change and the resulting radial ozone flux will decrease becoming eventually negligible as well.

Besides diffusion, advection also contributes to radial losses. In this study a gas flow rate of $F = 1$ L/m is considered, corresponding to a characteristic gas flow speed of $F/(2Rg) \sim 40$ cm/s. The advection loss ($S_{f,i}$) for O and O$_3$ are $\sim 2 \cdot 10^{18}$ cm^{-3} s^{-1} and $\sim 2 \cdot 10^{17}$ cm^{-3} s^{-1}, respectively. These are more than an order of magnitude smaller than the loss due to gas phase reactions (see Fig. 4(b) for O) and radial diffusion, and therefore advection can be neglected in this case. At higher flow rates, however, advection can become an important loss mechanism and it should be accounted for in the simulations.

B. Axial losses

Axial losses due to flux of species to the electrodes are important for two reasons. First they can affect the particle balance in the discharge and therefore the densities obtained in the plasma; and secondly, the flux of species to the electrodes represent the plasma dosage experienced by a target sample during a direct plasma treatment.

ROS such as O, O$_2$(a), and O$_3$ are considered key species for plasma functionalization and plasma medicine. At present, however, little information is found in the literature regarding the actual plasma dosage as this is difficult to quantify. This hinders the application of plasmas and their standardization.

Net axial losses are determined by incoming fluxes and surface reactions on the electrodes/target. These reactions, however, are difficult to predict and reaction rates are often unknown. For modelling purposes, we assume here that species

reaching the electrodes will be adsorbed with a certain probability p_i, regardless of what reaction they may undergo. Thus, for a given probability p_i the electrode loss for neutral species i is

$$EL_i = p_i\Gamma_i s_e/V, \tag{18}$$

where EL_i represents the electrode loss of species i in the unit of cm^{-3} s^{-1}, p_i the adsorption probability of species i, and s_e the total area of electrode-plasma interface. p_i is an adsorption/reaction probability with value between 0 and 1. To assess the influence of p_i on the net flux of species reaching the electrode, i.e., the plasma dosage, p_i is swept by
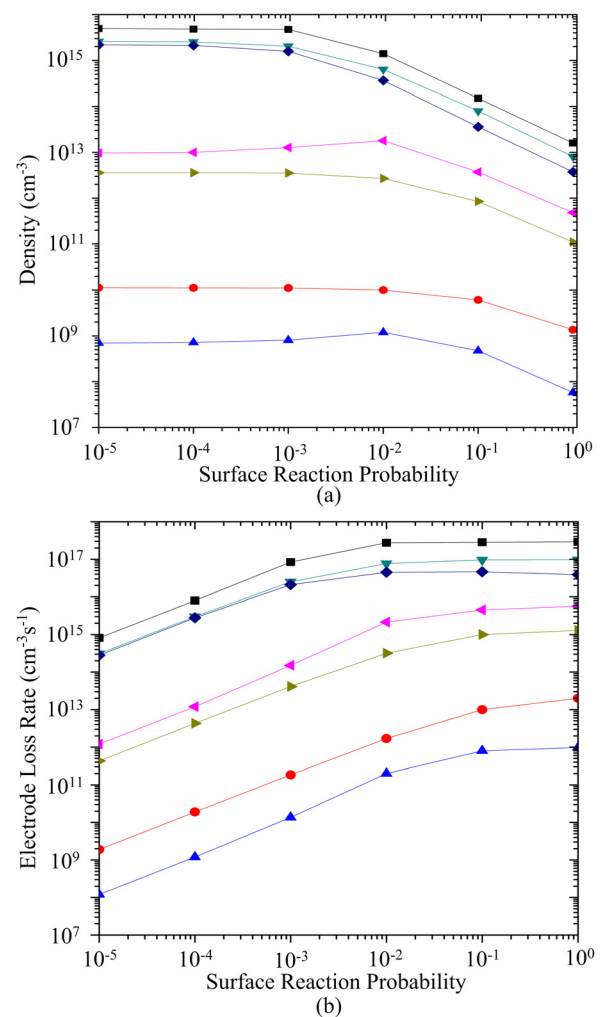

FIG. 7. (Color online) Time-averaged (a) densities and (b) electrode loss rate of ROS at plasma-electrode interface as a function of electrode absorption probability. ■: O; ●: O(^{1}d); ▲: O (^{1}s); ▼: O$_2$(a); ◄: O$_2$(b); ►: O$_2$(v); ◆: O$_3$.

5 orders of magnitude from 10^{-5} to 1. For simplicity, the same value of p_i is applied to all the species. The resulting time-averaged densities and fluxes of ROS at the plasma-electrode interface are shown in Fig. 7. For small values of p_i ($<10^{-3}$), the adsorption is negligible and it does not affect the density on the gas phase. For $p_i > 10^{-3}$, however, the loss at the electrode becomes significant and the density of species in the plasma-electrode interface decreases monotonically with increasing p_i. As a result, the electrode loss rate (EL_i) increase monotonically at very low values of p_i but it remains fairly constant for $p_i > 10^{-3}$. This result indicates that surface reactions are likely to be diffusion limited when $p_i > 0.001$ due to the large collisionality of the plasma. Therefore even if p_i is not known precisely, the plasma dosage can be estimated with reasonable accuracy because EL_i becomes fairly independent of p_i.

Even though electrode losses are negligible when compared with gas phase reactions (e.g., electrode loss rate of ground state O is $\sim 10^{17}$ cm^{-3} s^{-1}, 2 orders of magnitude lower than that of gas phase loss), electrode losses need to be taken into account in order to estimate the actual plasma dosage received by a target.

VI. CONCLUSIONS

A 1-dimensional computational study of atmospheric-pressure rf He+(0.5%) O$_2$ cold plasmas is presented. The fluid model used incorporates 17 species and 60 gas phase reactions, which had been identified as the main species and reactions in a previous study with a more comprehensive chemistry model (250+ reactions).

O_2^+, O_3^-, and O are the dominant positive ion, negative ion and reactive oxygen species, respectively. The plasma is electronegative with an electronegativity $\alpha \sim 1$ and double layers form at the sheath-bulk boundaries. Phase-averaged spatial profiles of all the species are presented. The plasma density is $\sim 10^{11}$ cm^{-3} and the main ROS (O) has a density of $\sim 10^{16}$ cm^{-3}. Ground state O is generated by electron induced reactions as well as the quenching of O* and O$_2$(b) by background gases, while the three-body reaction to form O$_2$ and O$_3$ are the main mechanism of O destruction. The simulation results are in good agreement with previous reports and experimental observations.

A power analysis indicates that 18% of the input power is coupled to ions. Besides the power coupled to positive ions as these are accelerated in the sheaths, >5% of the input power is dissipated by ions in the bulk. This amount will increase further as the electronegativity increases and therefore it should not be assumed that power in the bulk is only coupled to electrons in atmospheric-pressure electronegative plasmas.

Expressions to estimate the radial loss of neutral species in zero and one dimensional studies are developed and the importance of these losses in atmospheric pressure plasmas is discussed. Given the large collisionality, loss of particles is diffusion limited (D/R $<<$ v$_{th}$) and as a result, this loss is negligible for most species in the plasma. For long lived species such as ozone, however, this loss should be taken into account if plasma species are not allowed to build up in the surrounding environment.

As a result of the diffusion limited situation, electrode loss of neutral species is nearly independent of the surface adsorption probability p when $p > 0.001$. As a result, the electrode loss can be quantified even if p is unknown (as it is often the case in practical scenarios). This can be of great valuable for novel plasma applications like surface functionalization and plasma medicine for which surface reactions remain largely unknown.

Therefore we expect that the results presented in this paper lead to a better understanding of He+O$_2$ plasma dynamics and chemistry, provide relations for improved global models of atmospheric-pressure electronegative plasmas, and benefit the investigation of plasma surface interactions in emerging plasma medicine applications.

APPENDIX: CHEMICAL REACTIONS INCLUDED IN THE MODELS

The chemical reactions in He+O$_2$ atmospheric-pressure cold plasmas, including electron impact reactions, ion neutral reactions, recombination, Penning ionization, collisional relaxation *et al.*

TABLE II. Chemical reactions included in the models.

No.	Reaction[a]	Rate coefficient[b]	Reference
1	$e + He \rightarrow e + He$	$f(T_e)$	52
2	$e + O_2 \rightarrow e + O_2$	$f(T_e)$	53
3	$e + O_2 \rightarrow O_2^+ + 2e$	$f(T_e)$	54
4	$e + He \rightarrow e + He^*$	$f(T_e)$	52
5	$e + O \rightarrow O(^1S) + e$	$f(T_e)$	55
6	$e + O_2 \rightarrow 2O + e$	$f(T_e)$	56
7	$e + O_2 \rightarrow O(^1D) + O + e$	$f(T_e)$	54
8	$e + O_2 \rightarrow O(^1S) + O + e$	$f(T_e)$	57
9	$e + O_2 \rightarrow O_2(b) + e$	$f(T_e)$	53
10	$e + O_2 \rightarrow O_2(a) + e$	$f(T_e)$	53
11	$e + O_2 \rightarrow O_2(v) + e$	$f(T_e)$	52
12	$e + O_2 \rightarrow O + O^-$	$f(T_e)$	57
13	$e + O_2(a) \rightarrow O_2(b) + e$	$f(T_e)$	58
14	$e + O \rightarrow O(^1D) + e$	$f(T_e)$	55
15	$e + O_2(b) \rightarrow O + O^-$	$f(T_e)$	59
16	$e + O_3 \rightarrow O^- + O_2$	$f(T_e)$	57
17	$e + O_2 + O_2 \rightarrow O_2^- + O_2$	$2.26 \times 10^{-30}(T_g/300)^{-0.5}$	48
18	$e + O_2 + He \rightarrow O_2^- + He$	1×10^{-31}	60
19	$e + O_4^+ \rightarrow 2O_2$	$2.25 \times 10^{-7}T_e^{-0.5}$	61
20	$O_2^+ + O^- + M \rightarrow O_2 + O + M$	$2 \times 10^{-25}(T_g/300)^{-2.5}$	62
21	$O_2^+ + O_2^- + M \rightarrow 2O_2 + M$	$2 \times 10^{-25}(T_g/300)^{-2.5}$	61

TABLE II. *Continued*

No.	Reaction[a]	Rate coefficient[b]	Reference
22	$O_2^+ + O_3^- + M \rightarrow O_3 + O_2 + M$	$2 \times 10^{-25}(T_g/300)^{-2.5}$	61
23	$O_4^+ + O^- + M \rightarrow 2O_2 + O + M$	$2 \times 10^{-25}(T_g/300)^{-2.5}$	61
24	$O_4^+ + O_2^- + M \rightarrow 3O_2 + M$	$2 \times 10^{-25}(T_g/300)^{-2.5}$	61
25	$O_4^+ + O_3^- + M \rightarrow 2O_2 + O_3 + M$	$2 \times 10^{-25}(T_g/300)^{-2.5}$	61
26	$O^- + O \rightarrow O_2 + e$	$2.0 \times 10^{-10}(T_g/300)^{0.5}$	62
27	$O^- + O_2(b) \rightarrow O_2 + O + e$	$6.9 \times 10^{-10}(T_g/300)^{0.5}$	62
28	$O^- + O_2(a) \rightarrow O_3 + e$	$3 \times 10^{-10}(T_g/300)^{0.5}$	62
29	$O_2^- + O \rightarrow O_3 + e$	$1.5 \times 10^{-10}(T_g/300)^{0.5}$	62
30	$O_2^- + O_2(b) \rightarrow 2O_2 + e$	3.6×10^{-10}	63
31	$O^- + O_2 + M \rightarrow O_3^- + M$	$1.1 \times 10^{-30}(T_g/300)^{-1}$	64
32	$O_2^+ + 2O_2 \rightarrow O_4^+ + O_2$	$2.4 \times 10^{-30}(T_g/300)^{-3.2}$	61
33	$O_2^+ + O_2 + He \rightarrow O_4^+ + He$	$5.8 \times 10^{-31}(T_g/300)^{-3.1}$	65
34	$O_2^- + O \rightarrow O^- + O_2$	$1.5 \times 10^{-10}(T_g/300)^{0.5}$	62
35	$O_2^- + O_3 \rightarrow O_3^- + O_2$	$6 \times 10^{-10}(T_g/300)^{0.5}$	62
36	$O_3^- + O \rightarrow O_2^- + O_2$	$2.5 \times 10^{-10}(T_g/300)^{0.5}$	62
37	$O_4^+ + O \rightarrow O_2^+ + O_3$	3×10^{-10}	61
38	$O_4^+ + O_2 \rightarrow O_2^+ + 2O_2$	$3.3 \times 10^{-6}\left(\dfrac{T_g}{300}\right)^{-4}\exp\left(-\dfrac{5030}{T_g}\right)$	61
39	$O_4^+ + O_2(a) \rightarrow O_2^+ + 2O_2$	1×10^{-10}	61
40	$He^* + O_2 \rightarrow O_2^+ + He + e$	$2.54 \times 10^{-10}(T_g/300)^{0.5}$	62
41	$He_2^* + O_2 \rightarrow O_2^+ + 2He + e$	$1 \times 10^{-10}(T_g/300)^{0.5}$	66
42	$O(^1D) + O_2 \rightarrow O + O_2$	$4.8 \times 10^{-12}\exp(67/T_g)$	67
43	$O(^1D) + O_2 \rightarrow O + O_2(a)$	$1.6 \times 10^{-12}\exp(67/T_g)$	67
44	$O(^1D) + He \rightarrow O + He$	1.0×10^{-13}	62
45	$O(^1D) + O_3 \rightarrow 2O + O_2$	1.2×10^{-10}	62
46	$O(^1D) + O_3 \rightarrow 2O_2$	1.2×10^{-10}	62
47	$O(^1S) + O_2 \rightarrow O(^1D) + O_2$	$3.2 \times 10^{-12}\exp(-850/T_g)$	62
48	$O(^1S) + O_2 \rightarrow O + O_2$	$1.6 \times 10^{-12}\exp(-850/T_g)$	62
49	$O(^1S) + O_2(a) \rightarrow O + O_2$	1.1×10^{-10}	62
50	$O(^1S) + O_3 \rightarrow 2O_2$	4.63×10^{-10}	68
51	$He^* + 2He \rightarrow He_2^* + He$	2×10^{-34}	69
52	$O_2(b) + O_3 \rightarrow 2O_2 + O$	1.54×10^{-11}	62
53	$O_2(b) + O_3 \rightarrow O_2(a) + O_2 + O$	7×10^{-12}	62
54	$O_2(a) + O + He \rightarrow O_2 + O + He$	1×10^{-32}	56
55	$He + 2O \rightarrow He + O_2$	$1.3 \times 10^{-32}\left(\dfrac{T_g}{300}\right)^{-1}\exp\left(-\dfrac{170}{T_g}\right)$	60
56	$2O + O_2 \rightarrow O_3 + O$	$3.4 \times 10^{-34}\exp(345/T_g)$	70
57	$O + O_2 + He \rightarrow O_3 + He$	$1.1 \times 10^{-34}\exp(510/T_g)$	60
58	$O(^1D) + O_2 \rightarrow O + O_2(b)$	$2.56 \times 10^{-11}\exp(67/T_g)$	67
59	$He_2^* + M \rightarrow 2He + M$	1.5×10^{-15}	69
60	$O_2(v) + M \rightarrow O_2 + M$	$1 \times 10^{-14}(T_g/300)^{0.5}$	62

[a]He^* represents $He(2^3S)$ and $He(2^1S)$; He_2^* represents $He_2(a^3\sum_u^+)$. M represents the background gases helium and oxygen.

[b]Rate coefficients have units of cm^3 s^{-1} for two-body reactions and cm^6 s^{-1} for three-body reactions; T_e has units eV; T_g has units K; $f(T_e)$ indicates that the rate coefficient is obtained from EEDF using cross sections from indicated reference.

[1]M. G. Kong, G. Kroesen, G. Morfill, T. Nosenko, T. Shimizu, J. van Dijk, and J. L. Zimmermann, New J. Phys. **11**, 115012 (2009).

[2]G. Fridman, G. Friedman, A. Gutsol, A. B. Shekhter, V. N. Vasilets, and A. Fridman, Plasma Processes Polym. **5**, 503 (2008).

[3]F. Iza, G. J. Kim, S. M. Lee, J. K. Lee, J. L. Walsh, Y. T. Zhang, and M. G. Kong, Plasma Processes Polym. **5**, 322 (2008).

[4]R. Hackam and H. Akiyama, IEEE Trans. Dielectr. Electr. Insul. **7**, 654 (2000).

[5]A. Mfopara, M. J. Kirkpatrick, and E. Odic, Plasma Chem. Plasma Process. **29**, 91 (2009).

[6]M. Laroussi, IEEE Trans. Plasma Sci. **30**, 1409 (2002).

[7]X. Deng, J. J. Shi, and M. G. Kong, J. Appl. Phys. **101**, 074701 (2007).

[8]A. N. Bhoj and M. J. Kushner, Plasma Sources Sci. Technol. **17**, 035024 (2008).

[9]T. Suzuki, T. Saburi, R. Tokunami, H. Murata, and Y. Fujii, Thin Solid Films **506–507**, 342 (2006).

[10]P. Bruggeman and C. Leys, J. Phys. D: Appl. Phys. **42**, 053001 (2009).

[11]M. A. Malik, A. Ghaffar, and S. A. Malik, Plasma Sources Sci. Technol. **10**, 82 (2001).

[12]P. Bruggeman, F. Iza, D. Lauwers, and Y. A. Gonzalvo, J. Phys. D **43**, 012003 (2010).

[13]K. McKay, D. X. Liu, M. Z. Rong, F. Iza, and M. G. Kong, Appl. Phys. Lett. **99**, 091501 (2011).

[14]M. A. Lieberman and A. J. Lichtenberg, *Principles of Plasma Discharges and Materials Processing*, 2nd ed. (Wiley-VCH, New York, 2005).

[15]D. X. Liu, P. Bruggeman, F. Iza, M. Z. Rong, and M. G. Kong, Plasma Sources Sci. Technol. **19**, 025018 (2010).

[16]D. X. Liu, X. H. Wang, M. Z. Rong, F. Iza, M. G. Kong, and P. Bruggeman, Plasma Processes Polym. **7**, 846 (2010).

[17]G. Y. Park, H. W. Lee, G. Kim, and J. K. Lee, Plasma Processes Polym. **5**, 569 (2008).

[18]G. Y. Park, Y. J. Hong, H. W. Lee, J. Y. Sim, and J. K. Lee, Plasma Processes Polym. **7**, 281 (2010).

[19]D. Liu, F. Iza, and M. G. Kong, IEEE Trans. Plasma Sci. **36**, 952 (2008).

[20]D. Lee, J. M. Park, S. H. Hong, and Y. Kim, IEEE Trans. Plasma Sci. **33**, 949 (2005).

[21]G. Y. Park, Y. J. Hong, H. W. Lee, J. Y. Sim, and J. K. Lee, Plasma Processes Polym. **7**, 281 (2010).

[22]A. N. Bhoj and M. J. Kushner, J. Phys. D: Appl. Phys. **40**, 6953 (2007).

[23]Y. Sakiyama and D. B. Graves. J. Appl. Phys. **101**, 073306 (2007).

[24]Y. Sakiyama and D. B. Graves, Plasma Sources Sci. Technol. **18**, 025022 (2009).

[25]J. J. Shi and M. G. Kong, J. Appl. Phys. **97**, 23306 (2005).

[26]J. J. Shi and M. G. Kong, Appl. Phys. Lett. **87**, 201501 (2005).

[27]D. W. Liu, F. Iza, and M. G. Kong, Appl. Phys. Lett. **93**, 261503 (2008).

[28]D. W. Liu, F. Iza, and M. G. Kong, Appl. Phys. Lett. **95**, 031501 (2009).

[29]S. S. Yang, S. M. Lee, F. Iza, and J. K. Lee, J. Phys. D: Appl. Phys. **39**, 2775 (2006).

[30]G. J. M. Hagelaar, F. J. de Hong, and G. M. W. Kroesen, Phys. Rev. E **62**, 1452 (2000).

[31]P. F. Kurunczi, J. Guha, and V. M. Donnelly, Phys. Rev. Lett. **96**, 018306 (2006).

[32]H. W. Ellis, R. Y. Pai, E. W. McDaniel, E. A. Mason, and L. A. Viehland, At. Data Nucl. Data Tables **17**, 177 (1976).

[33]G. J. M. Hagelaar and L. C. Pitchford, Plasma Sources Sci. Technol. **14**, 722 (2005).

[34]R. Deloche, P. Monchicourt, M. Cheret, and F. Lambert, Phys. Rev. A **13**, 1140 (1976).

[35]J. E. Morgan and H. I. Schiff, Can. J. Chem. **42**, 2300 (1964).

[36]G. S. Timmins, E. J. H. Bechara, and H. M. Swartz, J. Exp. Biol. **203**, 2479 (2000).

[37]A. V. Ivanov, S. Trakhtenberg, A. K. Bertram, Y. M. Gershenzon, and M. J. Molina, J. Phys. Chem. A **111**, 1632 (2007).

[38]A. J. Lichtenberg, Y. T. Lee, M. A. Lieberman, I. D. Kaganovich, and L. D. Tsendin, Plasma Sources Sci. Technol. **6**, 437 (1997).

[39]J. P. Boeuf, Phys. Rev. A. **36**, 2782 (1987).

[40]D. Ellerweg, J. Benedikt, A. von Keudell, N. Knake, and V Schulz-von der Gathen, New J. Phys. **12**, 013021 (2010).

[41]B. Halliwell and J. M. C. Gutteridge, *Free Radicals in Biology and Medicine*, 4th ed. (Clarendon, Oxford, 2007).

[42]P. Bruggeman and D. C. Schram, Plasma Sources Sci. Technol. **19**, 045025 (2010).

[43]G. Koo, J. H. Cho, and W. M. Lee, Plasma Processes Polym. **5**, 161 (2008).

[44]J. Park, I. Henins, H. W. Herrmann, G. S. Selwyn, J. Y. Jeong, R. F. Hicks, D. Shim, and C. S. Chang, Appl. Phys. Lett. **76**, 288 (2000).

[45]X. T. Deng, J. J. Shi, and M. G. Kong, J. Appl. Phys. **101**, 074701 (2007).

[46]C. Lee and M. A. Lieberman, J. Vac. Sci. Technol. A **13**(2), 368 (1995).

[47]S. Kim, M. A. Lieberman, and A. J. Lichtenberg, J. Vac. Sci. Technol. A **24**(6), 2025 (2006).

[48]J. T. Gudmundsson, I. G. Kouznetsov, K. K. Patel, and M. A. Lieberman, J. Phys. D: Appl. Phys. **34**, 1100 (2001).

[49]J. T. Gudmundsson and E. G. Thorsteinsson, Plasma Sources Sci. Technol. **16**, 399 (2007).

[50]D. D. Monahan and M. M. Turner, Plasma Sources Sci. Technol. **17**, 045003 (2008).

[51]X. Yuan and Laxminarayan L. Raja, IEEE Trans. Plasma Sci. **31**, 495 (2003).

[52]BOLSIG + software version 1.1. 2008 http://www.siglo-kinema.com/technical.htm (accessed April 2010).

[53]Y. Itikawa, A. Ichimura, K. Onda, K. Sakimoto, K. Takayanagi, Y. Hatano, M. Hayashi, M. Nishimura, and S. Tsurubuchi, J. Phys. Chem. Ref. Data **18**, 23 (1989).

[54]B. Eliasson and U. Kogelschatz, Report No. KLR-86-11C, Brown Boveri Forschungszentrum CH-5405 Baden, 1986.

[55]R. R. Laher and F. R. Gilmore, J. Phys. Chem. Ref. Data **19**, 277 (1990).

[56]A. A. Ionin, I. V. Kochetov, A. P. Napartovich, and N. N. Yuryshev, J. Phys. D: Appl. Phys. **40**, R25 (2007).

[57]J. W. McConkey, C. P. Malone, P. V. Johnson, C. Winstead, V. McKoy, and I. Kanik, Phys. Rep. **466**, 1 (2008).

[58]R. I. Hall and S. Trajmar, J. Phys. B **8**, L293 (1975).

[59]S. L. Akhmanov, K. S. Klopovskiy, and A. P. Osipov, Manuscript 5472-83 deposited in VINITI, Moscow (in Russian), 1983.

[60]K. R. Stalder, R. J. Vidmar, G. Nersisyan, and W. G. Graham, J. Appl. Phys. **99**, 093301 (2006).

[61]I. A. Kossyi, A. Y. Kostinsky, A. A. Matveyev, and V. P. Silakov, Plasma Sources Sci. Technol. **1**, 207 (1992).

[62]D. S. Stafford and M. J. Kushner, J. Appl. Phys. **96**, 2451 (2004).

[63]F. J. Gordillo-Vazquez, J. Phys. D: Appl. Phys. **41**, 234016 (2008).

[64]R. J. Vidmar and K. R. Stalder, Computations of the power to sustain plasma in air with relevance to aerospace technology, Final report prepared for Air Force Office of Scientific Research, Report No. AFRLS-RARRE040123, Contract No. F49620-01-1-0414. Feb. 20, 2004.

[65]A. Good, Chem. Rev. **75**, 561 (1975).

[66]R. P. Cardoso, T. Belmonte, G. Henrion, and N. Sadeghi, J. Phys. D: Appl. Phys. **39**, 4178 (2006).

[67]R. Atkinson, D. L. Baulch, R. A. Cox, R. F. Hampson, Jr., J. A. Kerr, M. J. Rossi, and J. Troe, J. Phys. Chem. Ref. Data **26**, 52 (1997).

[68]NIST chemical kinetic database, http://kinetics.nist.gov/kinetics/index.jsp, accessed April 2010.

[69]Y. B. Golubovskii, V. A. Maiorov, J. Behnke, and J. F. Behnke, J. Phys. D: Appl. Phys. **36**, 39 (2003).

[70]S. Hadi-Ziane, B. Held, and P. Pignolet, J. Phys. D: Appl. Phys. **25**, 677 (1992).